

# The effects of pyridine derivative additives on interface processes at nanocrystalline TiO<sub>2</sub> thin film in dye-sensitized solar cells

Xiong Yin,<sup>1,4</sup> Hui Zhao,<sup>2,4</sup> Liping Chen,<sup>3,4</sup> Weiwei Tan,<sup>1,4</sup> Jingbo Zhang,<sup>1</sup> Yuxiang Weng,<sup>2</sup> Zhigang Shuai,<sup>3</sup> Xurui Xiao,<sup>1</sup> Xiaowen Zhou,<sup>1</sup> Xueping Li<sup>1</sup> and Yuan Lin<sup>1\*</sup>

<sup>1</sup> Key Laboratory of Photochemistry, Beijing National Laboratory for Molecular Sciences (BNLMS), Institute of Chemistry, Chinese Academy of Sciences, Beijing 100080, China

<sup>2</sup> Laboratory of Soft Matter Physics, Beijing National Laboratory and Condensed Matter Physics, Institute of Physics, Chinese Academy of Sciences, Beijing 100080, China

<sup>3</sup> Key Laboratory of Organic Solids, Institute of Chemistry, Chinese Academy of Sciences, Beijing 100080, China

<sup>4</sup> Graduate School of the Chinese Academy of Sciences, Beijing 100039, China

Received 21 May 2007; Revised 18 July 2007; Accepted 25 July 2007

2-Methyl-4-propoxypyridine, a new pyridine derivative, has been synthesized and used as an additive in the liquid electrolyte of dye-sensitized solar cells (DSSCs). Compared with 2-methylpyridine and 4-*tert*-pyridine, they were employed to study the influence of the pyridine derivative additives on the rate of recombination at the electrode/dye/electrolyte interfaces and band edge shift of TiO<sub>2</sub>, which were measured by time-resolved mid-infrared absorption spectroscopy and Mott–Schottky analysis, respectively. It was found that the rate of interfacial charge recombination was enhanced when the pyridine derivative additives were present in the electrolyte. Meanwhile, the additives caused a negative shift of the band edge. However, the net effect of pyridine derivative addition was to improve the open-circuit photovoltage according to the photoelectrochemical measurement, indicating that negative shift of conduction band of TiO<sub>2</sub> was a predominant factor in improving the open-circuit photovoltage. Also, the result was strongly supported by the dark current measurement. Therefore, it provides a microscopic account for the function of the pyridine derivative additives on the open-circuit photovoltage enhancement of the DSSCs. Furthermore, the decrease of the short-circuit photocurrent of the cells was also attributed to the slower dye regeneration due to the addition of additives from the results of cyclic voltammetry measurement. Copyright © 2007 John Wiley & Sons, Ltd.

**KEYWORDS:** dye-sensitized solar cell; pyridine derivative additives; photovoltage enhancement; back electron transfer

## INTRODUCTION

During the past decades, dye-sensitized nanocrystalline TiO<sub>2</sub> solar cells (DSSCs) constructed by using nanocrystalline metal oxides, typically TiO<sub>2</sub>, dye molecules and liquid electrolytes have attracted much attention because of their attractive features of high energy conversion efficiency and low production cost.<sup>1–6</sup> Under light irradiation, electrons in the dye are excited and injected into the conduction band of the nanocrystalline metal oxides, and the injected electrons transmit to the conductive substrate. The resulting oxidized dye cations are reduced by the redox couple in the electrolyte. The open-circuit photovoltage ( $V_{oc}$ ), one of the energy conversion parameters of the cell, is thermodynamically determined by the difference between the electron quasi-Fermi level in the TiO<sub>2</sub> film under illumination and the

redox potential of the redox couple in the electrolyte.<sup>7–9</sup> In dynamic processes, there are two possible factors that influence the  $V_{oc}$ :<sup>10</sup> one is the charge recombination at the TiO<sub>2</sub> electrode/redox electrolyte interfaces, and the other is the band edge shift of TiO<sub>2</sub> with respect to the redox potential of the electrolyte. Smestad reported that a  $V_{oc}$  of over 1 V was possible for Ru complexes at AM 1.5 by using detailed energy balance calculations.<sup>11</sup> However, the practical value of  $V_{oc}$  is always smaller than the expected theoretical maximum. In order to gain an acceptable  $V_{oc}$ , the charge transfer at the electrode/dye/electrolyte interfaces in DSSCs should be adjusted to suppress the charge recombination. Palomares *et al.* investigated the effect of three metal oxide overlays, SiO<sub>2</sub>, Al<sub>2</sub>O<sub>3</sub> and ZrO<sub>2</sub>, on the charge recombination, whose conduction band edges are significantly negative with respect to the TiO<sub>2</sub> conduction band edge, resulting in a physical barrier layer for charge recombination.<sup>12</sup> Meanwhile, Nb<sub>2</sub>O<sub>5</sub> coated on TiO<sub>2</sub> nanoporous electrode working as a blocking layer has been studied by Chen *et al.*<sup>13</sup> Wang and coworkers

\*Correspondence to: Yuan Lin, Laboratory of Photochemistry, Beijing National Laboratory for Molecular Sciences (BNLMS), Institute of Chemistry, Chinese Academy of Sciences, Beijing 100080, China. E-mail: Linyuan@iccas.ac.cn

demonstrated that co-grafting an amphiphilic ruthenium dye with hexadecylmalonic acid<sup>14</sup> or 1-decylphosphonic acid<sup>15</sup> on a TiO<sub>2</sub> semiconductor nanocrystal remarkably enhanced the photocurrent, photovoltage and conversion efficiency of DSSCs. The enhancement was ascribed to the formation of a hydrophobic spacer between TiO<sub>2</sub> and the electrolyte, which provides a more effective insulating barrier for the back electron transfer from the TiO<sub>2</sub> conduction band to the triiodide in the electrolyte. Also, Kroeze *et al.*<sup>16</sup> found that efficient retardation of charge recombination in electrolyte can be achieved by the application of recombination-blocking amphiphilic alkyl chains attached to the sensitizer dye, resulting in a significantly improved device performance. Huang *et al.*<sup>7</sup> demonstrated that treating dye-coated TiO<sub>2</sub> electrodes with pyridine derivatives, such as 2-vinylpyridine and poly(2-vinylpyridine), can improve significantly both the  $V_{oc}$  and the photon-to-electricity conversion efficiency of the cell, and the increase in the  $V_{oc}$  correlates to a decrease in the back electron transfer rate by one to two orders in magnitude. Kopidakis and coworkers<sup>17</sup> studied the effect of adsorbent guanidinium on the  $V_{oc}$  of the DSSCs, and found that after adding guanidinium to the solution, the recombination between electron in the conduction band and  $I_3^-/I^-$  become slower and the band edge moves positively, resulting in an improvement in the  $V_{oc}$ . Therefore, the employed methods to improve  $V_{oc}$  can be summarized as follows: (i) depositing a metal oxide on the TiO<sub>2</sub> surface to retard the charge recombination; (ii) establishing a hydrophobic spacer between TiO<sub>2</sub> and the electrolyte to reduce back electron transfer; (iii) adding small organic molecules to the electrolyte to shift the band edge of TiO<sub>2</sub> negatively or positively. Meanwhile, much effort has been made to understand the mechanism of how the pyridine derivatives influence the  $V_{oc}$  of the DSSCs. Kusama *et al.*<sup>18</sup> investigated the influence of some nitrogen-containing compounds on the performance of DSSCs using a density functional theory (DFT) method. They reported that a more efficient charge transfer between the nitrogen-containing compounds and iodine molecules would occur when the  $V_{oc}$  value is increased. Grätzel and coworkers<sup>19</sup> have reported that adding 4-*tert*-pyridine (4-TBP) to the  $I_3^-/I^-$  redox electrolyte in the acetonitrile increased the  $V_{oc}$  and solar cell performance, which was attributed to the adsorption of 4-TBP at the bare TiO<sub>2</sub> surface. It is caused by the interaction between the Ti(IV) ion, which has Lewis acidity and the lone electron pair of the nitrogen atom of 4-TBP. The oxygen atom in some organic molecules, such as dimethyl sulfoxide and tetrahydrofuran, has lone electron pair and its effect on  $V_{oc}$  have been investigated by Fukui *et al.*<sup>20</sup>

In this paper, we report the synthesis of 2-methyl-4-propoxyppyridine (4-POP) with two coordination sites in the molecule, as an additive in liquid electrolyte, and investigated its influence on interfacial processes at TiO<sub>2</sub> thin films in DSSCs, in comparison with 4-TBP and 2-methylpyridine (2-MP). The three different additives result in the different performance of DSSCs because of their different chemical structures. The Mülliken atomic charges of the three pyridine derivative additives have been calculated with

DFT. Time-resolved mid-infrared absorption spectroscopy, a new powerful technique that can be used to detect the conduction band and the trapped electrons directly, is applied to study the rate of back electron transfer at the electrode/dye/electrolyte interfaces. The flat band potential of TiO<sub>2</sub> thin film electrode (essentially the conduction band edge movement) is examined by the Mott–Schottky analysis method, and the effect of the above-mentioned two factors on  $V_{oc}$  is also discussed in detail. Moreover, the reason for decline of short-circuit photocurrent density is investigated by cyclic voltammetry (CV) measurements.

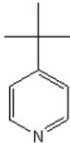
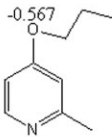
## EXPERIMENTAL

### Chemicals

2-MP, 4-TBP and 3-methoxypropionitrile (MPN) were purchased from Aldrich, and distilled under vacuum prior to use. Lithium iodide (Aldrich) and iodine (Aldrich) were used without further purification. 4-POP (structure shown in the Fig. 1) was synthesized from 2-MP and 1-propanol. The detailed synthesis method will be published elsewhere,<sup>21</sup> and its structure and purity were examined by <sup>1</sup>H-NMR, infrared spectroscopy and mass spectroscopy. The standard electrolyte for DSSCs was composed of 0.5 M LiI and 0.05 M I<sub>2</sub> in MPN. Meanwhile, the three pyridine derivative additives at two concentrations, 0.1 and 0.5 M, were added into the standard electrolyte.

### Preparation of dye-sensitized TiO<sub>2</sub> thin film

The conducting glass substrate (fluorine-doped tin oxide glass (FTO), ~20 Ω/sq) was ultrasonically cleaned and rinsed with water and 2-propanol, then soaked in the 2-propanol for at least 24 h. The FTO substrate was dried under a nitrogen stream prior to film preparation. The nanoporous TiO<sub>2</sub> electrode was prepared according to the following process. A colloidal TiO<sub>2</sub> suspension was prepared by the hydrolysis of titanium isopropoxide precursor in pH = 2 acetic acid aqueous solution under vigorous stirring at 80 °C. The suspension was then autoclaved at 250 °C and concentrated in a rotary evaporator. The TiO<sub>2</sub> suspension was deposited onto conductive glass sheets using the 'doctor blade method'. After the sample was air-dried, the plate was sintered at 450 °C for 30 min in air to form a nanoporous film. The thickness of the TiO<sub>2</sub> film was about 15 μm determined using cross-sectional FE-SEM. A 5 × 10<sup>-4</sup> M solution of *cis*-di(thiocyanato)-*N,N'*-bis(2,2'-bipyridyl-4,4'-dicarboxylic acid) ruthenium (II) (N3) in absolute ethanol was used to sensitize the nanoporous

structure			
atomic charge	-0.365	-0.403	-0.409
name	4- <i>tert</i> -butylpyridine	2-methylpyridine	2-methyl-4-propoxyppyridine
abbr.	4-TBP	2-MP	4-POP

**Figure 1.** The name, structure and atomic charge of the pyridine derivative additives used in this study.

film. The fresh nanoporous TiO<sub>2</sub> film was dipped into the dye solution while its temperature was above 80 °C, and then kept in the solution for 12 h at room temperature. The physically adsorbed dye was removed by the subsequent rinsing of the electrode with absolute ethanol. The dye-sensitized TiO<sub>2</sub> films were immediately used in the photoelectrochemical measurement.

### Photoelectrochemical and electrochemical measurements

The 2-electrode sandwich cell for photovoltaic measurement consisted of a dye-sensitized TiO<sub>2</sub> electrode, an organic electrolyte containing triiodide and iodine and a counter electrode. The platinized, semitransparent counter electrode was prepared by thermal decomposition of 5 mM H<sub>2</sub>PtCl<sub>6</sub> in 2-propanol on a conducting glass plate at 390 °C for 15 min.<sup>22</sup> The counter electrode and dye-sensitized TiO<sub>2</sub> electrode were clamped firmly together and redox electrolyte solution was introduced into the porous structure of the TiO<sub>2</sub> film by capillary action.<sup>19</sup> The cell was illuminated through the dye-sensitized TiO<sub>2</sub> film. The active area was 0.2 cm<sup>2</sup>. The photovoltaic performances of the DSSCs were recorded with a PAR potentiostat (Model 273). A 300 W Xe arc lamp (Oriol) together with optical filters was used as the light source for simulating the solar spectrum at AM 1.5 (100 mW cm<sup>-2</sup>). The dark current measurement of the cell was conducted in a dark box with the same PAR potentiostat.

The flat band potential of TiO<sub>2</sub> nanocrystalline film electrode was measured by the Mott–Schottky analysis method.<sup>23,24</sup> The Mott–Schottky analysis was performed on a Solartron SI1287 electrochemical interface and Solartron 1255B frequency response analyzer with the potential range from 0 to -1.5 V, using the three-electrode system in standard electrolyte with or without additives. The TiO<sub>2</sub> film electrode was used as the working electrode, a Pt foil as the counter electrode and a saturated calomel electrode (SCE) as the reference electrode.

The CV measurements were carried out on a Solartron SI1287 electrochemical interface at a scanning rate of 50 mV/s.<sup>5</sup> A dye-coated FTO conductive glass electrode was prepared by immersing the conductive glass substrate, which was heated at 120 °C for 1 h, into 5 × 10<sup>-4</sup> M N3 ethanol solution for 12 h. A thin-layer three-electrode electrochemical cell was constituted with a dye-coated FTO conductive glass as the working electrode and a platinized FTO conductive glass whose conductive surface was split to two parts, one part as the counter electrode and the other as the reference electrode.

### Time-resolved mid-infrared absorption measurement

For time-resolved mid-IR measurements, the TiO<sub>2</sub> nanocrystalline film deposited on the CaF<sub>2</sub> substrate (25 mm diameter, 3 mm thick windows) was dipped into the dye solution at 40 °C, and then kept for 12 h at room temperature. The electrolyte solution was dropped on the dye-sensitized TiO<sub>2</sub> film, which was pressed tightly against by another CaF<sub>2</sub> plate, then placed in a stainless steel chamber and sealed airtight with O-rings. No light bias or external potential was applied on the CaF<sub>2</sub> plates. The 532 nm excitation pulse was

generated by a Nd:YAG laser (Spectra Physics Co., Lab 170, repetition rate: 10 Hz, pulse width: 10 ns). The mid-IR probe beam was generated by a liquid-N<sub>2</sub>-cooled cw CO laser (made in Dalian University of Technology, China), which was tunable from 5.0 to 6.5 μm with a spectral spacing around 4 cm<sup>-1</sup>. The 532 nm excitation pulse energy was 0.63 mJ/pulse, and the size of the defocused IR beam was about 3 mm in diameter. The transmitted IR probe beam was detected by a mercury cadmium telluride (MCT) detector (Kolmar Technology, Model: KV104-0.5-A-3/8), and its photocurrent output was amplified by a current preamplifier (Kolmar Technology, Model: KA020-A1) and filtered by a low-band-pass filter (20 MHz–DC). Finally, the signal was acquired by a digital oscilloscope (Tektronix TDS500D) and the data was transferred to a personal computer. The transient response in absorbance as small as 10<sup>-4</sup> was detected by signal-averaging 300 laser shots.<sup>25–27</sup>

### The theoretical calculations of atomic charge

The theoretical calculations were performed with DFT implemented in the Gaussian 03 package.<sup>28</sup> The molecular structures are optimized at the hybrid DFT levels by B3LYP functions, which combine Becke's three-parameter exchange functional (B3)<sup>29,30</sup> with the correlation functional of Lee, Yang, and Parr (LYP).<sup>31</sup> A basis set of 6-31g<sup>32</sup> is used.

## RESULTS AND DISCUSSION

### The photovoltaic performance of DSSCs

Table 1 shows the effects of pyridine derivative additives in the liquid electrolyte on performance of N3-sensitized TiO<sub>2</sub> solar cell under 100 mW cm<sup>-2</sup> irradiation. It is found that after the addition of different pyridine derivatives at two concentrations, 0.1 and 0.5 M, *V*<sub>oc</sub> of the cell dramatically increased from 0.45 V to above 0.60 V. Among three pyridine derivative additives, 4-POP showed the largest *V*<sub>oc</sub> (0.736 V) and the lowest *J*<sub>sc</sub> (10.14 mA cm<sup>-2</sup>) at the concentration of 0.5 M. As for 0.5 M 4-TBP, it showed the third largest *V*<sub>oc</sub> (0.703 V) and a much higher *J*<sub>sc</sub> (15.20 mA cm<sup>-2</sup>), resulting in the highest efficiency among all tested solar cells. Table 1 also displays that *J*<sub>sc</sub> decreases with the increasing *V*<sub>oc</sub>. In addition, for the same pyridine derivative additive, it is found that value of *V*<sub>oc</sub> at an additive concentration of 0.5 M was higher than at 0.1 M, while the *J*<sub>sc</sub> showed a contrary trend. For example, *J*<sub>sc</sub> and *V*<sub>oc</sub> of 0.1 M 2-MP in

**Table 1.** Effect of pyridine derivative additives on the photovoltaic properties of dye-sensitized TiO<sub>2</sub> solar cell

Additives	<i>V</i> <sub>oc</sub> (V)	<i>J</i> <sub>sc</sub> (mA cm <sup>-2</sup> )	FF	η (%)
None	0.445	18.75	0.53	4.41
0.1 M 4-TBP	0.618	16.32	0.59	5.96
0.1 M 2-MP	0.624	15.72	0.62	6.07
0.1 M 4-POP	0.644	13.71	0.67	5.92
0.5 M 4-TBP	0.703	15.20	0.63	6.73
0.5 M 2-MP	0.711	14.32	0.66	6.70
0.5 M 4-POP	0.736	10.14	0.69	5.08

electrolyte were  $15.72 \text{ mA cm}^{-2}$  and  $0.624 \text{ V}$ , respectively. As the concentration of 2-MP was  $0.5 \text{ M}$ , they were  $14.32 \text{ mA cm}^{-2}$  and  $0.711 \text{ V}$ , respectively.

### Interfacial carrier relaxation dynamics of TiO<sub>2</sub> dye-sensitized film in electrolyte

To investigate the influence on the rate of back electron transfer, i.e., the injected electrons on the TiO<sub>2</sub> conduction band recombine with redox pair in electrolyte,<sup>19</sup> after the additives were added into the electrolyte, we employed the time-resolved mid-IR absorption spectroscopy to study the back electron transfer between the injected electrons on the conduction band of N3-sensitized TiO<sub>2</sub> film and electrolyte with different additives.<sup>25–27,33–35</sup> Fig. 2 displays the temporal profile of transient absorption probed at  $1800 \text{ cm}^{-1}$  of N3-sensitized TiO<sub>2</sub> with three different pyridine derivative additives of  $0.5 \text{ M}$  in the electrolyte. The kinetics detected at other wavelengths is basically similar. Strong absorption decay due to photogenerated electrons in the conduction band of TiO<sub>2</sub> is observed. The decay curves are fitted by a biexponential equation, and the fitted decay components together with the corresponding pre-exponential factors are listed in Table 2. The values of  $\tau_1$  (fast component) and  $\tau_2$  (slow component) listed in Table 2 represent electron-decay lifetime in the conduction band of TiO<sub>2</sub>. The decay time constant  $\tau_1$  of the fast component means that the electrons on the conduction of TiO<sub>2</sub> recombine more quickly with the acceptor in the electrolyte, which makes the  $V_{oc}$  decline. However, the decay time constant  $\tau_2$  of the slow component means that more electrons will stay in conduction band, leading to an improvement of  $V_{oc}$ . Furthermore, the increase of the conduction band of TiO<sub>2</sub> may prevent the electrons injecting from the LUMO of N3 to the conduction band of TiO<sub>2</sub> according to the Frank–Condon

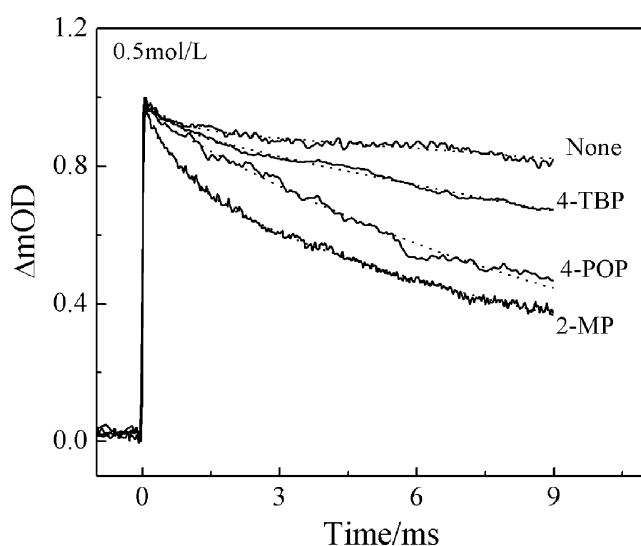


**Figure 2.** The temporal profiles of transient absorption of N3-sensitized TiO<sub>2</sub> film without any additive or with three different additives in the electrolyte probed at  $1800 \text{ cm}^{-1}$ , after the excitation by the  $532 \text{ nm}$  laser pulse. Additives include 4-TBP, 4-POP and 2-MP. Solid lines: experimental curves; dotted lines: fitting curves. The concentration of additives was  $0.5 \text{ M}$ , and the energy was  $0.63 \text{ mJ/pluse}$ .

**Table 2.** The fitting parameters obtained from the fitting curves in Figs 2 and 3

Additive	$\tau_1$ (ms)	$A_1$	$\tau_2$ (ms)	$A_2$	$\tau_1 \times \tau_2$
None	0.59	0.33	84.50	3.50	49.86
0.1 M 4-TBP	0.65	0.58	40.26	7.35	26.17
0.1 M 2-MP	1.01	0.88	24.10	12.77	24.34
0.1 M 4-POP	0.29	0.30	20.46	9.95	5.93
0.5 M 4-TBP	0.55	0.61	32.83	10.99	18.06
0.5 M 2-MP	0.87	1.47	11.64	5.14	10.12
0.5 M 4-POP	0.11	0.49	11.12	6.35	1.22

principle, which may reduce the number of electrons on the conduction of TiO<sub>2</sub>.  $\tau_1$  and  $\tau_2$  show the different behaviors on  $V_{oc}$ . Moreover, their influence on  $V_{oc}$  are complicated. Yanagida *et al.*<sup>36</sup> have proposed that the conversion efficiency of DSSC is determined partly by efficiency of electron ( $\eta_e$ ), which can be described by the following equation,

$$\eta_e = \eta_{ei} \times \eta_{et} \times \eta_{ec} \quad (1)$$

where  $\eta_{ei}$ ,  $\eta_{et}$ , and  $\eta_{ec}$  represent efficiency of electron injection, transport and collection respectively. Since both  $\tau_1$  and  $\tau_2$  in Table 2 can represent the character of electron related to the  $V_{oc}$  and they show the different behaviors on  $V_{oc}$ , the effective factor would be better expressed by the empirical relation, i.e.,  $\tau_1 \times \tau_2$ , in parallel to  $\eta_{ei} \times \eta_{et} \times \eta_{ec}$ . The principle underlying this relation is not clear, yet. And it is under further investigation.

It can be seen from Table 2 that the decay rate of electrons in the conduction band is enhanced by the addition of  $0.5 \text{ M}$  pyridine derivatives, which means a fast back electron transfer compared with the electrolyte without any pyridine derivatives (noted as 'None'). The rate of back electron transfer decreases in the order of 4-POP > 2-MP > 4-TBP > None. Figure 3 shows the decay of two concentrations for three different pyridine derivative additives (the fitting data are also listed in Table 2), which displays the effect of the concentration of the pyridine derivative additives on the rate of back electron transfer. For all pyridine derivatives,  $\tau_1 \times \tau_2$  at a high concentration was smaller than that at a low concentration, which means that the rate of back electron transfer in the high concentration was faster than that in the low concentration. It can be also seen from Table 2 that the rate of back electron transfer for  $0.1 \text{ M}$  decreases in the order of 4-POP > 2-MP > 4-TBP > None, the same as the concentration of  $0.5 \text{ M}$ .

### Flat band potential of the TiO<sub>2</sub> electrode

We evaluated the flat band potential  $V_{fb}$  of TiO<sub>2</sub> electrode in different electrolytes by using the Mott–Schottky analysis method. The method involves measuring different capacitances as a function of the applied potential. The relationship between the capacitance and the applied potential can be expressed by the following equation:

$$\frac{1}{C_{sc}^2} = \frac{2 \left( |E - E_{fb}| - \frac{kT}{e} \right)}{\epsilon \epsilon_0 e N_D} \quad (2)$$

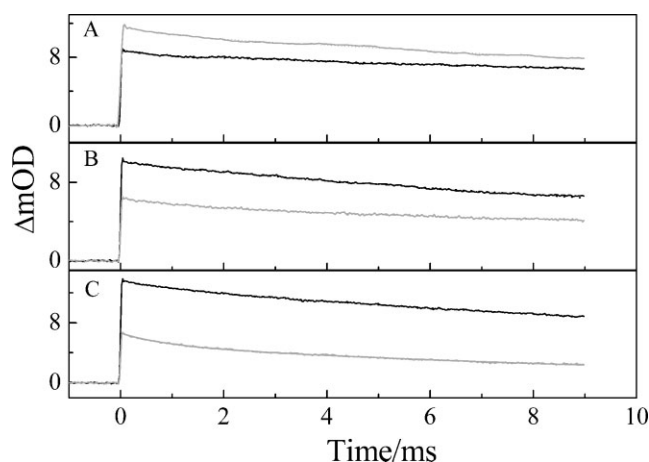


**Figure 3.** The temporal profiles of transient absorption of N3-sensitized TiO<sub>2</sub> film with three different pyridine derivative additives of two concentrations in the electrolyte, probed at 1800 cm<sup>-1</sup>, after the excitation by the 532 nm laser pulse. Additives include: (A) 4-TBP, (B) 4-POP and (C) 2-MP. Solid lines: experimental curves; Dotted lines: fitting curves; Black: 0.1 M. Light gray: 0.5 M.  $\Delta OD = \log(I_{out}/I_{in})$  with  $I_{out}$  and  $I_{in}$  being the output and incident optical intensities, and the energy was 0.63 mJ/pluse.

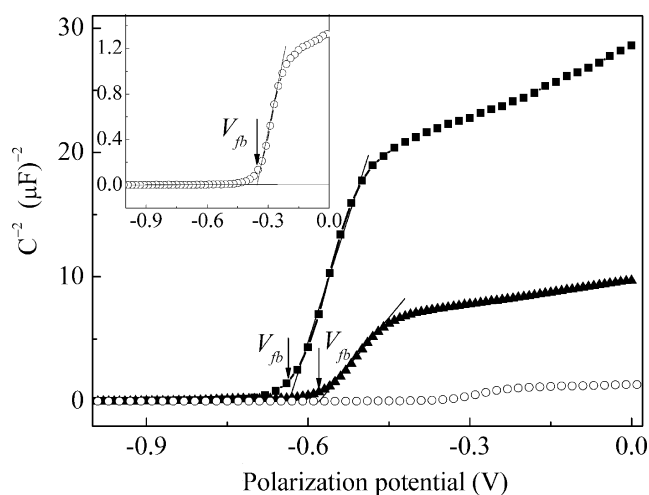


**Figure 4.** Mott-Schottky curves for TiO<sub>2</sub> film in the electrolyte without any additive or with 0.1 M additives versus the applied potential with respect to the saturation calomel electrode: None (hollow circle); 4-TBP (full triangle); 4-POP (full square). The inset shows the curve in the electrolyte without additive.

where  $C_{sc}$  is the space-charge capacitance,  $\epsilon$  is the dielectric constant of the semiconductor,  $\epsilon_0$  is the permittivity of free space,  $N_D$  is the dopant density,  $E_{fb}$  is the flat band potential and  $E$  is the applied potential. Figure 4 shows the typical Mott-Schottky curves versus applied potential for TiO<sub>2</sub> film in the electrolyte containing 0.1 M 4-POP and 0.1 M 4-TBP. The inset shows the plot for the TiO<sub>2</sub> film in the electrolyte without the additive. The plot of  $1/C_{sc}$  versus the applied potential shows an X-intercept corresponding to  $V_{fb}$ . The deviation from linearity may result from the effect of surface states, recombination effects and non-negligible contributions of the Helmholtz layer to

**Table 3.** Flat band potential of TiO<sub>2</sub> ( $V_{fb}$ ) and changes in  $V_{fb}$  ( $\Delta V_{fb}$ ) and  $V_{oc}$  ( $\Delta V_{oc}$ ) of dye-sensitized solar cells before and after addition of pyridine derivative additives

Additives	$V_{fb}$ (V Vs SCE)	$\Delta V_{fb}$ (V)	$\Delta V_{oc}$ (V)
None	-0.376	0.000	0.000
0.1 M 4-TBP	-0.580	-0.204	0.173
0.1 M 2-MP	-0.611	-0.235	0.179
0.1 M 4-POP	-0.635	-0.259	0.199
0.5 M 4-TBP	-0.644	-0.268	0.258
0.5 M 2-MP	-0.655	-0.279	0.266
0.5 M 4-POP	-0.699	-0.323	0.291

the interfacial capacitance.<sup>37</sup> Table 3 summarizes the effects of pyridine derivatives on  $V_{fb}$ . The value of  $V_{fb}$  for each additive at the same concentration decreased in the order of 4-POP > 2-MP > 4-TBP > None. After the addition of pyridine derivative additives to the electrolyte,  $V_{fb}$  shifted to a more negative value for all pyridine derivatives. A higher concentration of the pyridine derivative additives gives rise to a more negative potential.

Obviously, there was a dramatic improvement on  $V_{oc}$  after the additives were added into the electrolyte according to the Table 1. One of the possible explanations for the improvement of  $V_{oc}$  can be related to the negative shift of the  $V_{fb}$  of the TiO<sub>2</sub> electrode in the different electrolytes. In an attempt to investigate the relationship between the  $V_{oc}$  and  $V_{fb}$ , we used the difference value of  $V_{oc}$  and  $V_{fb}$  in the electrolyte with pyridine derivative additives with respect to those without pyridine derivative additives. It can be concluded from the Table 3 that the  $\Delta V_{oc}$  was smaller than the corresponding  $\Delta V_{fb}$  for the same pyridine derivative additives. In addition, another factor to affect the  $V_{oc}$  is the back electron transfer at the electrode/dye/electrolyte interfaces. According to the Marcus-Gericher theory,<sup>38,39</sup> the interfacial transfer rate constant from the conduction band to the redox species in the electrolyte is expressed by the equation:

$$k_{et} = \delta v_{th} \sigma \left[ \frac{kT}{\pi \lambda} \right]^{1/2} \exp \left( - \frac{(E_{redox} - \lambda - E_{cb})^2}{4 \lambda kT} \right) \quad (3)$$

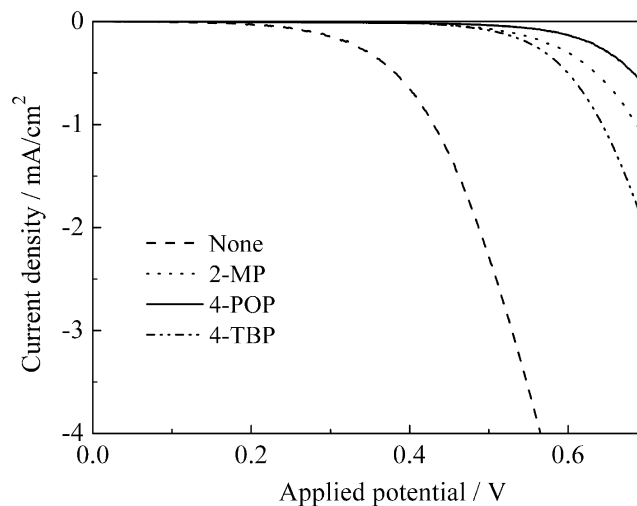
where  $\delta$  is the reaction layer thickness for interfacial electron transfer,  $v_{th}$  is the thermal velocity of the electron,  $\sigma$  is the reaction cross section and  $\lambda$  is the solvent reorganization energy. When conduction band of TiO<sub>2</sub> shifts negatively, the driving force increases for the charge recombination from the conduction to the redox in electrolyte, resulting in the enhancement of the rate of back electron transfer, and thus the decrease of  $V_{oc}$ . Frank *et al.*<sup>17</sup> have reported that some additives, such as ammonia, caused the band to move negatively and recombination to increase, the effect of which was to improve  $V_{oc}$ . Therefore, we believe that the  $\Delta V_{oc}$  was smaller than  $\Delta V_{fb}$ , which is in part due to the enhancement of back electron transfer after addition of each pyridine derivatives.

Figure 2 also shows that the rate of back electron transfer decreased in the order of 4-POP > 2-MP > 4-TBP > None, which is good agreement with the order of  $V_{fb}$  for

each additives. Furthermore, we used DFT<sup>28–32</sup> to calculate the atomic charge distribution on each pyridine derivative additives. The analyses of Mülliken atomic charges were performed on the optimized structures obtained at the B3LYP/6-31g level. In Fig. 1, the selected Mülliken atomic charges (also known as partial charges) of the molecules are listed. According to the result, it is believed that the atomic charge distribution of nitrogen atom of the pyridine derivatives is influenced by their structures. Compared with 4-TBP (−0.365), a much larger partial charge in 2-MP (−0.403) is due to the more electron-donating extent for 2-positional substitution by methyl group than that of 4-positional substitution by *tert*-butyl group. The 4-POP with two coordination sites shows almost the same partial charge (−0.409) with the 2-MP on the nitrogen atom, but its oxygen atom shows the largest partial charge (−0.567) among them resulting from 4-positional propoxylation. Grätzel and coworkers<sup>19</sup> have reported that adsorption of 4-TBP at the TiO<sub>2</sub> surface is caused by interaction between the Ti(IV) ion, which has Lewis acidity, and the lone electron pair of 4-TBP. Therefore, the larger the partial charge on the nitrogen or oxygen atom of the pyridine derivative additives is, the easier and the more often the pyridine derivations can be adsorbed onto the Lewis acid sites of the bare TiO<sub>2</sub> surface, which would cause a larger  $V_{oc}$  by negative shifting of the conduction band edge of TiO<sub>2</sub>.<sup>20</sup> According to Table 2, for all pyridine derivatives, the rate of back electron transfer for high concentration was faster than that at low concentration. The higher the concentration the pyridine derivatives was, the easier and more often pyridine could be adsorbed onto the Lewis acid site of TiO<sub>2</sub>, which led to the fast rate of back electron transfer. On light irradiation, the dyes adsorbed on the TiO<sub>2</sub> particles inject electrons into the conduction band, and the conduction band of the TiO<sub>2</sub> electrode dramatically shifts toward negative, especially after pyridine derivative additives were added.<sup>3</sup> The negative shift of the conduction band enhances the driving force for the recombination at the interface between the electron in the conduction band and  $I_3^-/I^-$  in the electrolyte, leading to a decrease of  $V_{oc}$  according to the Marcus–Gericher theory. Moreover,  $V_{oc}$  is enhanced after the addition of various derivatives according to Table 3. It is clear that the negative shift of the conduction band edge of TiO<sub>2</sub> is the predominant factor on the change of  $V_{oc}$ . Therefore, we compared the interface charge recombination rate with  $V_{fb}$  as various additives, giving a mechanistic account of the function of the additives to improve the  $V_{oc}$  of DSSCs.

### The dark current measurement

The dark current arises from the reduction of triiodide by conduction band electrons.<sup>19</sup> According to the Fig. 5, it can be found that the dark current diminished after 0.5 M pyridine derivative was added. The dark current decreases in the order of None > 4-TBP > 2-MP > 4-POP. The small dark current leads to a large  $V_{oc}$ .<sup>19,40</sup> The corresponding  $V_{oc}$  should follow the order: 4-POP > 2-MP > 4-TBP > None. It is obvious that the results of photoelectrochemical measurement are consistent with the order according to Table 1. With the addition of pyridine



**Figure 5.** Dark current–voltage curves obtained for DSSCs based on N3 dye without any additive or with 0.5 M various pyridine derivative additives in MPN containing 0.5 M LiI and 0.05 M I<sub>2</sub>: None (dashed line), 4-TBP (dashed-dotted-dotted line), 2-MP (dotted line), 4-POP (solid line).

derivative additives, it has been assumed that the adsorption of additive increases the distance between the TiO<sub>2</sub> and I<sub>3</sub><sup>−</sup>.<sup>41</sup> In other words, the dark current is restrained after the addition of pyridine derivatives. The dark current is a qualitative measure of interface charge recombination at the dye-sensitized TiO<sub>2</sub> in DSSCs.<sup>19</sup> And the measurement does not readily distinguish between passivation or activation of TiO<sub>2</sub> surface and band edge movement.<sup>17</sup> Therefore, the dark current measurement is an apparent analysis on the interface charge recombination, and provides a net effect of additive on the photovoltage of DSSCs. The results of dark current experiment strongly support the conclusion that the negative shift of the conduction band edge of TiO<sub>2</sub> is the predominant factor determining the  $V_{oc}$ .

### Analysis of short-circuit current by CV

Under irradiation, the potential drop in the Helmholtz layer depends on absorbed molecules,<sup>42,43</sup> and the different pyridine derivative additives will result in different potentials of the conduction band edge of the TiO<sub>2</sub> nanoporous film. Moreover, it is believed that when the conduction band shifts negatively, the driving force for the electron injection process from the LUMO of N3 into the conduction band of TiO<sub>2</sub> decreases, leading to low injection efficiency and a small photocurrent. In addition, the photocurrent is also determined by the dye regeneration process. For further analyzing the effect of pyridine derivative additives, the dye regeneration reaction ( $3I^- + 2Dye^+ \rightarrow I_3^- + 2Dye$ ) taking place at nanocrystalline TiO<sub>2</sub> electrode interface was studied by CV measurement.

CV is a powerful tool in analyzing the relationship between ion diffusivity and reaction kinetics of an electrochemical system.<sup>44</sup> The aim of this study was to examine the kinetic impediment of the I<sub>3</sub><sup>−</sup>/I<sup>−</sup> redox reaction in the case of different additives. Figure 6 illustrates the cyclic voltammograms obtained in electrolytes with different pyridine derivative additive of 0.5 M under the scanning range of 0 to

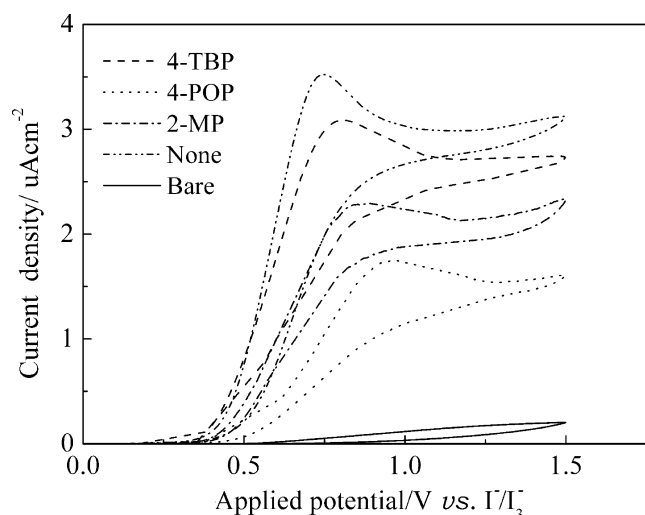


**Figure 6.** Cyclic voltammetry for the dye-coated FTO electrode in the electrolyte containing 0.5 M LiI, 0.05 M I<sub>2</sub> without any additives or with 0.5 M additives: None (dashed-dotted-dotted line); 4-TBP (dashed line); 2-MP (dashed-dotted line); 4-POP (dotted line); None using the bare FTO electrode (solid line). Scanning rate: 50 mV/s.

+1.5 V (versus I<sub>3</sub><sup>-</sup>/I<sup>-</sup>). The voltammograms show the anodic peaks, which cannot be observed for the bare FTO electrode, assigned to anodic oxidization of iodide by oxidized dye. The anodic peak potential shifts negatively and the peak current density gradually decreases in the order of None > 4-TBP > 2-MP > 4-POP. The cathodic peak cannot be presented in this scanning range, implying the irreversible behavior of this electrochemical reaction at N3-coated FTO electrode. The negative shifts of anodic peak potential and the increases of anodic peak current density shown in the voltammogram indicate that in the electrolyte a faster dye regeneration results in a higher *J*<sub>sc</sub>, which may lead to a different photocurrent due to different pyridine derivative additives added into electrolytes.

## CONCLUSIONS

Three pyridine derivatives were employed as additives in MPN electrolyte containing 0.5 M LiI and 0.05 M I<sub>2</sub>. Pyridine derivative additives with large partial charge enhance the open-circuit voltage, but usually reduces the short-circuit photocurrent density. Results from time-resolved mid-IR spectroscopy and the Mott-Schottky analysis method demonstrate that the increase in photovoltage is generated from the negative shift the conduction band of TiO<sub>2</sub> nanocrystalline, as well as the increase of back electron transfer from the conduction band of TiO<sub>2</sub> to the triiodide in the electrolyte primarily resulting from enhancing the driving force for recombination due to the addition of three pyridine derivatives into the MPN. However, the improvement of interface recombination and the negative shift of the conduction band edge produces a net photovoltage enhancement of about 0.29 V in the case of 0.5 M 4-POP, indicating that the negative shift of the conduction band edge of TiO<sub>2</sub> is the predominant factor in increasing *V*<sub>oc</sub>. The dark current measurement strongly supports the above-mentioned result. The driving

force for the electron injection process decreases owing to the negative shifting of the conduction band, which leads to a small photocurrent after addition of different additives to electrolyte. The decline of *J*<sub>sc</sub> may also be attributed to the slow dye regeneration according to the CV measurement.

## Acknowledgements

This work is support by Nation Research Fund for Fundamental Key Project (2006CB202605) and Nation Natural Science Foundation of China (50221201 and 50473055). Experimental help from Shujing Feng and Hanping Zhang is gratefully acknowledged. Thanks are due to Qiqiang Wang and Min Liu for help with the synthesis.

## REFERENCES

- O'Regan B, Grätzel M. *Nature* 1991; **353**: 737, DOI:10.1038/353737a0.
- Hagfeldt A, Grätzel M. *Chem. Rev.* 1995; **95**: 49.
- Grätzel M. *Nature* 2001; **414**: 338, DOI:10.1038/35104607.
- Kuang DB, Klen C, Snaith HJ, Moser J-E, Humphry-Baker R, Comte P, Zakeeruddin SM, Grätzel M. *Nano Lett.* 2006; **6**: 769, DOI: 10.1021/nl060075m.
- Wang M, Xiao XR, Zhou XW, Li XP, Lin Y. *Sol. Energy Mater. Sol. Cells* 2007; **91**: 785, DOI:10.1016/j.solmat.2007.01.009.
- Li MY, Feng SJ, Fang SB, Xiao XR, Li XP, Zhou XW, Lin Y. *Electrochim. Acta* 2007; **52**: 4858, DOI:10.1016/j.electacta.2007.01.027.
- Huang SY, Schlichthorl G, Nozik AJ, Grätzel M, Frank AJ. *J. Phys. Chem. B* 1997; **101**: 2576, DOI: 10.1021/jp962377q.
- Schiff EA. *Sol. Energy Mater. Sol. Cells* 2003; **78**: 567, DOI:10.1016/S0927-0248(02)00452-X.
- Frank AJ, Kopidaksi N, Lagemaat VD. *Coord. Chem. Rev.* 2004; **248**: 1165.
- Schlichthorl G, Huang SY, Sprague J, Frank AJ. *J. Phys. Chem. B* 1997; **101**: 8141, DOI: 10.1021/jp9714126.
- Smestad G. *Sol. Energy Mater. Sol. Cells* 1994; **32**: 273.
- Palomares E, Clifford JN, Haque SA, Lutz T, Durrant JR. *J. Am. Chem. Soc.* 2003; **125**: 475, DOI: 10.1021/ja027945w.
- Chen SG, Chappel S, Diamant Y, Zaban A. *Chem. Mater.* 2001; **13**: 4629, DOI: 10.1021/cm010343b.
- Wang P, Zakeeruddin SM, Comte P, Charvet R, Humphry-Baker R, Grätzel M. *J. Phys. Chem. B* 2003; **107**: 14336, DOI: 10.1021/jp0365965.
- Wang P, Zakeeruddin SM, Humphry-Baker R, Moser JE, Grätzel M. *Adv. Mater.* 2003; **15**: 2101.
- Kroeze JE, Hirata N, Koops S, Nazeeruddin MdK, Schmidt-Mende L, Grätzel M, Durrant JR. *J. Am. Chem. Soc.* 2006; **128**: 16376, DOI: 10.1021/ja065653f.
- Kopidaksi N, Neale NR, Frank AJ. *J. Phys. Chem. B* 2006; **110**: 12485, DOI: 10.1021/jp0607364.
- Kusama H, Sugihara H. *Sol. Energy Mater. Sol. Cells* 2006; **90**: 953, DOI:10.1016/j.solmat.2005.05.014.
- Zakeeruddin MK, Kay A, Rodicio I, Humphry-Baker R, Muller E, Liska P, Vlachopoulos N, Grätzel M. *J. Am. Chem. Soc.* 1993; **115**: 6382.
- Fukui A, Komiya R, Yamanaka R, Isiam A, Han LY. *Sol. Energy Mater. Sol. Cells* 2006; **90**: 649, DOI:10.1016/j.solmat.2005.01.020.
- Yin X, Tan WW, Zhang JB, Xiao XR, Zhou XW, Li XP, Lin Y. Submitted to *Surf. Interface Anal.*
- Wang GQ, Lin Y, Xiao XR, Li XP, Wang WB. *Surf. Interface Anal.* 2004; **36**: 1437, DOI: 10.1002/sia.1905.
- Wang M, Zhang QL, Weng YX, Lin Y, Xiao XR. *Chin. Phys. Lett.* 2006; **23**: 724.
- Redmond G, Fitzmaurice D. *J. Phys. Chem.* 1993; **97**: 1426.
- Ghosh HN, Asbury JB, Weng YX, Lian T. *J. Phys. Chem. B* 1998; **102**: 10208, DOI: 10.1021/jp983502w.
- Weng YX, Wang YQ, Asbury JB, Ghosh HN, Lian T. *J. Phys. Chem. B* 2000; **104**: 93, DOI: 10.1021/jp992522a.
- Zhao H, Zhang QL, Weng YX. *J. Phys. Chem. C* 2007; **111**: 3762, DOI: 10.1021/jp0645566.

28. Frisch MJ, Trucks GW, Schlegel HB, Scuseria GE, Robb MA, Cheeseman JR, Montgomery JA, Jr, Vreven T, Kudin KN, Burant JC, Millam JM, Iyengar SS, Tomasi J, Barone V, Mennucci B, Cossi M, Scalmani G, Rega N, Petersson GA, Nakatsuji H, Hada M, Ehara M, Toyota K, Fukuda R, Hasegawa J, Ishida M, Nakajima T, Honda Y, Kitao O, Nakai H, Klene M, Li X, Knox JE, Hratchian HP, Cross JB, Bakken V, Adamo C, Jaramillo J, Gomperts R, Stratmann RE, Yazyev O, Austin AJ, Cammi R, Pomelli C, Ochterski JW, Ayala PY, Morokuma K, Voth GA, Salvador P, Dannenberg JJ, Zakrzewski VG, Dapprich S, Daniels AD, Strain MC, Farkas O, Malick DK, Rabuck AD, Raghavachari K, Foresman JB, Ortiz JV, Cui Q, Baboul AG, Clifford S, Cioslowski J, Stefanov BB, Liu G, Liashenko A, Piskorz P, Komaromi I, Martin RL, Fox DJ, Keith T, Al-Laham MA, Peng CY, Nanayakkara A, Challacombe M, Gill PMW, Johnson B, Chen W, Wong MW, Gonzalez C, Pople JA. *Gaussian 03*. Gaussian: Pittsburgh, 2003.
29. Becke AD. *J. Chem. Phys.* 1993; **98**: 5648.
30. Becke AD. *Phys. Rev. A* 1988; **38**: 3098.
31. Lee C, Yang W, Paar RG. *Phys. Rev. B* 1980; **37**: 785.
32. Hehre WJ, Ditchfield R, Pople JA. *J. Chem. Phys.* 1972; **56**: 2257.
33. Takeshita K, Sasaki Y, Kobashi M, Tanaka Y, Maeldal S, Yamakata A, Ishibashi T, Onishi H. *J. Phys. Chem. B* 2003; **107**: 4156, DOI: 10.1021/jp0275645.
34. Takeshita K, Sasaki Y, Kobashi M, Tanaka Y, Maeldal S, Yamakata A, Ishibashi T, Onishi H. *J. Phys. Chem. B* 2004; **108**: 2963, DOI: 10.1021/jp035416o.
35. Heimer TA, Heilweil EJ. *J. Phys. Chem. B* 1997; **101**: 10990, DOI: 10.1021/jp972560z.
36. Hattori S, Hasobe T, Ohkubo K, Urano Y, Umezawa N, Nagano T, Wada Y, Yanagida S, Fukuzumi S. *J. Phys. Chem. B* 2004; **108**: 15200, DOI: 10.1021/jp047656p.
37. Cordon F, Gome WP. *Ber. Bunsenges. Phys. Chem.* 1976; **80**: 475.
38. Marcus RA. *Can. J. Chem.* 1959; **37**: 155.
39. Marcus RA. *J. Chem. Phys.* 1956; **24**: 966.
40. Hara K, Dan-oh Y, Kasada C, Ohga Y, Shinpo A, Suga S, Sayama K, Arakawa H. *Langmuir* 2004; **20**: 4205, DOI: 10.1021/la0357615.
41. Nakade S, Kanzaki T, Kubo W, Kitamura T, Wada Y, Yanagida S. *J. Phys. Chem. B* 2005; **109**: 3480, DOI: 10.1021/jp0460036.
42. Liu Y, Hagfeldt A, Xiao XR, Lindquist SE. *Sol. Energy Mater. Sol. Cells* 1998; **55**: 267.
43. Lyon LA, Hupp JT. *J. Phys. Chem.* 1995; **99**: 15718.
44. Papageorgiou N, Maier WF, Grätzel M. *J. Electrochem. Soc.* 1997; **144**: 876.